Asian Journal of Chemistry; Vol. 36, No. 11 (2024), 2539-2546

ASIAN JOURNAL OF CHEMISTRY

https://doi.org/10.14233/ajchem.2024.32491

Synthesis, Characterization, Photocatalytic and Self Cleaning Behaviour of Sepiolite-Supported $CdFe_2O_4$ Nanocomposite

K. KALPANA and K. RAJATHI*

PG and Research Department of Chemistry, Kalaignar Karunanidhi Government Arts College (Affiliated to Thiruvalluvar University, Vellore), Tiruvannamalai-606603, India

*Corresponding author: E-mail: rajathi_sridhar@rediffmail.com

Received: 9 August 2024; *Accepted*: 10 October 2024; *Published online*: 30 October 2024; AJC-21787

This study employed the hydrothermal co-precipitation approach to synthesize several natural clay-sepiolite supported cadmium ferrite ($CdFe_2O_4$) photocatalysts with different weight percentages of sepiolite (3, 5, 9 wt.%). Several techniques were used to characterize the sepiolite/$CdFe_2O_4$ composite like photoluminescence spectroscopy (PL), diffuse reflectance spectroscopy (DRS), scanning electron microscopy (SEM), high-resolution transmission electron microscopy (HR-TEM) and BET surface area analysis. The results showed that improved $CdFe_2O_4$ with 5 wt.% sepiolite had superior photocatalytic activity than undoped $CdFe_2O_4$ in eliminating azo dye rhodamine-B when exposed to solar light. The sandwich-like microstructure is shown loosely clustering together in FE-SEM images, with an average particle size of about 50 nm. Moreover, the BET results showed that sepiolite/$CdFe_2O_4$ has a larger surface area than undoped $CdFe_2O_4$. $CdFe_2O_4$, supported by sepiolite, remarkably indicated good photocatalytic activity for up to four applications in a row. Sepiolite/$CdFe_2O_4$ is characterized by a high degree of hydrophobicity, as shown by a contact angle of 108.3º and this hydrophobic property is useful for making materials that clean themselves.

Keywords: Sepiolite, Cadmium ferrite, Photocatalytic activity, Self cleaning behaviour, BET surface area analysis.

INTRODUCTION

Nowadays researchers have focused on the preparation of cadmium ferrite ($CdFe_2O_4$) because of its various applications in many industries [1,2]. Ferrites are a class of metal oxides that mainly consist of iron oxides. Its optical, magnetic and electrical properties allow them to be applied in a multitude of ways, for example, photodegradation of industrial wastes or dyes [3], the degradation of organic pollutants through piezo-electric catalysis [4,5], components of battery electrodes [6], materials used in solar cell windows [7] and biological systems, such as bioimaging [8] and magnetic resonance imaging as well as nanomaterials with both luminescent and magnetic properties [9], either paramagnetic or ferromagnetic.

The tetrahedral (A) and octahedral (B) sites of cadmium ferrite nanoparticles, a representative of the general spinel ferrite system, are filled with non-magnetic (Cd^{2+}) ions coordinated with magnetic (Fe^{3+}) ions [10,11]. The literature provides reports on a variety of synthetic methods for producing spinel-ferrite nanoparticles. Solid state reaction [12], sol-gel process [13], combustion synthesis [14], sonochemical technique [15], electro-chemical method [16], hydrothermal method [17], precursor route [18], co-precipitation [19], microemulsions [20], reverse micelles [21], solvothermal method [22], ball milling [23] and microwave processing [24] are the few well-known methods. The adsorption of organic dyes and metals from aqueous solutions has been implemented in recent years using naturally occurring clay minerals such as bentonite, montmorillonite, palygorskite, kaolinite and sepiolite [25-33].

Sepiolite [$Si_{12}Mg_8O_{30}(OH)_4(H_2O)_4{\cdot}8H_2O$], a magnesium phyllosilicate, consists of two tetrahedral layers of silica and a layer of magnesium ions with octahedral coordination. Sepiolite exhibits infinite channels with a cross-section of 0.4 nm^2 in size, similar to other phyllosilicates where the octahedron sheets are not constant [34-36]. TiO_2, Fe_2O_3, Na_2O, MgO, SiO_2, CaO, K_2O, Al_2O_3 and many other metals and metal oxides are found in sepiolite clay [37]. Excellent ion exchange and adsorption performance have been provided by this type of

clay mineral due to its unique micromorphology and nanoscale pores [38].

For the production of inorganic and metal-based nanoparticles, co-precipitation is a simple process with a controllable size distribution, high yield and an environmental friendly solvent. Due to these advantages, it is decided to synthesize sepiolite-supported $CdFe_2O_4$ nanocomposite by employing hydrothermal co-precipitation method and evaluated its photocatalytic activity by using solar light to remove rhodamine-B dye and also examined its hydrophobic properties.

EXPERIMENTAL

Ferric nitrate nonahydrate ($Fe(NO_3)_3{\cdot}9H_2O$), cadmium acetate dihydrate ($Cd(CH_3COO)_2{\cdot}2H_2O$), sodium hydroxide and ethanol were of AR-grade purity (99% purity) and supplied by Himedia Chemicals. Rhodamine-B dye (*m.f.* $C_{28}H_{31}N_2O_3Cl$, *m.w.*: 479.01) was supplied by Colour Chem, Pondicherry, India. Himedia Chemicals supplied the sepiolite clay and washed thoroughly to eliminate the impurities. Distilled water was used throughout the experiments.

Characterization: Using a Siemens D5005 diffractometer and Cu*K*α (k = 0.151418 nm) radiation, the X-ray diffraction (XRD) patterns were analyzed. The diffractograms were recorded with count duration of 20 s and in a 2θ range between 10º and 80º. Using a Model ULTRA-55 field emission scanning electron microscope (FE-SEM), the morphology of nanocomposite was investigated. To capture images at different magnifications, samples were positioned on a gold platform inside the scanning electron microscope. A 200 kV ultra high-resolution transmission electron microscope (JEOL-2010) equipped with a Leica high-resolution optical microscope was used to capture HR-TEM images. A tiny quantity of catalyst solution was applied to a thin layer of copper grids with holes in them covered with carbon. The grids were checked and then allowed to air dry. The diffuse reflectance spectra of every catalyst were recorded using a Shimadzu UV 2450 model fitted with an integrating sphere, with powdered $BaSO_4$ as a reference. The Perkin-Elmer LS 55 fluorescence spectrometer was used to record the photoluminescence (PL) spectrum at room temperature. The surface area of nanocomposite was ascertained using a Micromeritics ASAP 2020 sorption analyzer. Using N_2 gas as adsorbate, the samples were analyzed at 77K following a 12 h degassing period at 423 K. The least-squares fit of the Brunauer-Emmett-Teller (BET) multipoint technique was employed to ascertain the specific surface area. A German made drop-shaped analyzer (DSA) manufactured by Kruss GmbH was used to record the contact angle in order to assessed the hydrophobicity of the nanocomposite.

Preparation of 5 wt.% sepiolite/$CdFe_2O_4$: Both pure $CdFe_2O_4$ and $CdFe_2O_4$ supported 5 wt.% sepiolite were prepared using the hydrothermal co-precipitation technique. The first step involved dissolution of 0.5 M of $Fe(NO_3)_3{\cdot}9H_2O$ and 0.3 M of $Cd(CH_3COO)_2{\cdot}2H_2O$ separately in 50 mL of distilled water. After mixing the above two solutions, 10 mL of ethanol and 0.5 g of sepiolite powder were added while being stirred constantly containing one drop of 0.2 M NaOH. The resulting solution was stirred at 80 ºC for 5 h. The final product was cleaned with ethanol followed by distilled water and then dried at 100 ºC for 5 h. The $CdFe_2O_4$ nanoparticles supported by sepiolite were labelled as sepiolite/$CdFe_2O_4$ following a 6 h calcination at 700 ºC. Similarly, pure $CdFe_2O_4$ nanoparticles were prepared using a method akin to this one, which did not need the use of sepiolite powder.

Photocatalytic degradation studies: The photocatalytic degradation were carried out in the summer from 11 a.m. to 2 p.m. under direct sunlight. A clear, 20 mm diameter borosilicate glass tube measuring 40 cm in height served as the reaction vessel in this experiment. The dye and sepiolite/$CdFe_2O_4$ solutions attained equilibrium between the adsorption and desorption processes after 0.5 h of magnetic stirring in a dark atmosphere. A 50 mL dye solution containing sepiolite/$CdFe_2O_4$ was continuously aerated using a pump to ensure complete mixing of the reaction solution and to add oxygen. During illumination, the solvent evaporation was negligible; concurrently, the initial sample was obtained in darkness while the adsorption process occurred. At regular intervals, a 2 mL sample was centrifuged and diluted to 10 mL volume. The sunlight intensity was measured with the LT Lutron LX-10/A Digital Lux metre.

RESULTS AND DISCUSSION

Powder XRD studies: The PXRD pattern of 5 wt.% sepiolite/$CdFe_2O_4$ reveals that the synthesized sample has tetrahedral phases of $CdFe_2O_4$ (JCPDS card No. 54-0964 and 22-1063) and rhombohedral phases of α-Fe_2O_3 (JCPDS card No. 79-1741) [39]. In Fig. 1b, the diffraction peaks at 25.86º, 32.74º, 36.45º and 41.85º for the planes (012), (104), (002) and (113), respectively. The 2θ values observed at 32.15º, 34.51º, 38.62º, 49.12º, 52.32º and 62.35º correspond to the (111), (311), (200), (024), (422) and (511) diffraction planes of CdO [40], whereas the 2θ values at 30.25º, 35.91º, 37.41º, 43.13º, 55.40º, 62.17º and 66.76º correspond to (220), (311), (222), (400), (220), (103) and (311) planes of tetrahedral phases of $CdFe_2O_4$ [41].

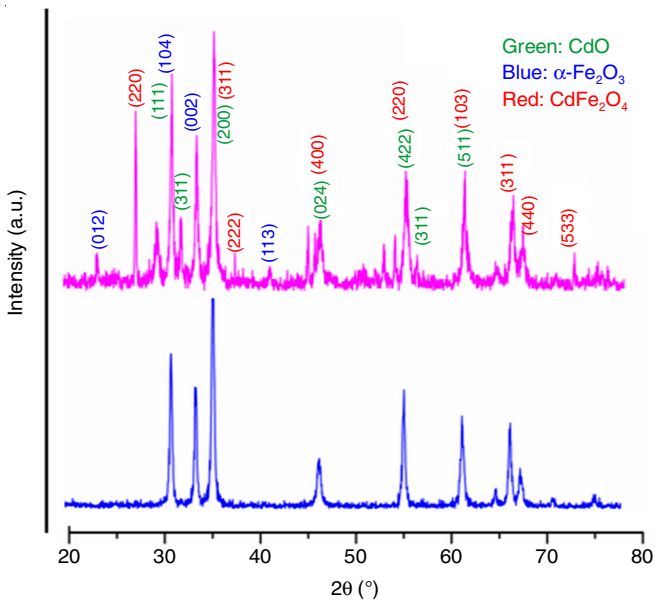

Fig. 1. XRD patterns of (a) prepared $CdFe_2O_4$ (b) prepared 5 wt% sepiolite/$CdFe_2O_4$

In addition, no evidence of additional crystalline defects and the diffraction peaks have not changed appreciably. The other new peaks shown in Fig. 1b confirm the presence of sepiolite clay particles. There are no visible crystallographic defects and no additional diffraction peaks have changed significantly. The average crystallite size of sepiolite/$CdFe_2O_4$ is determined from the Scherrer's equation to be 24.5 nm.

FE-SEM studies: The FE-SEM images of 5 wt.% sepiolite/$CdFe_2O_4$ at different magnifications and locations are shown in Fig. 2. The FE-SEM images of sepiolite/$CdFe_2O_4$ exhibited the sandwich-like microstructure loosely clustering together and the average size of particles is about 50 nm. The porous structures of randomly oriented nanocomposites can also produce nanoflakes and help the dye molecules bind to catalyst surfaces. The particles in the sepiolite/$CdFe_2O_4$ samples have smooth surfaces and irregular forms. Moreover, several tiny particles are clearly visible on the surface of sepiolite clay.

HR-TEM studies: At low-magnification, the TEM images of sepiolite/$CdFe_2O_4$ (Fig. 3a-d) revealed a large number of regular shaped hollow spherical-like particles with a diameter of below 50 nm, which further proves that $CdFe_2O_4$ nanoparticles are uniformly deposited on the surface of the sepiolite clay surface.

Diffuse reflectance spectral (DRS) studies: The fundamental absorption edge of tetrahedral $CdFe_2O_4$ rises at 430 nm, which is attributed to its intrinsic band gap of 2.95 eV. Fig. 4 displays the prepared $CdFe_2O_4$ (Fig. 4b) and sepiolite/$CdFe_2O_4$ (Fig. 4a) diffuse reflectance spectra in the reflectance mode. In the UV and visible spectrum, 5 wt.% $CdFe_2O_4$ shows reduced reflectance (increased absorbance) in contrast to $CdFe_2O_4$ and sepiolite/$CdFe_2O_4$. Incorporation of sepiolite loading helps $CdFe_2O_4$ to better absorb the visible range of 400 to 800 nm, which proves that sepiolite/$CdFe_2O_4$ can be used as a UV and visible light active semiconductor photocatalyst.

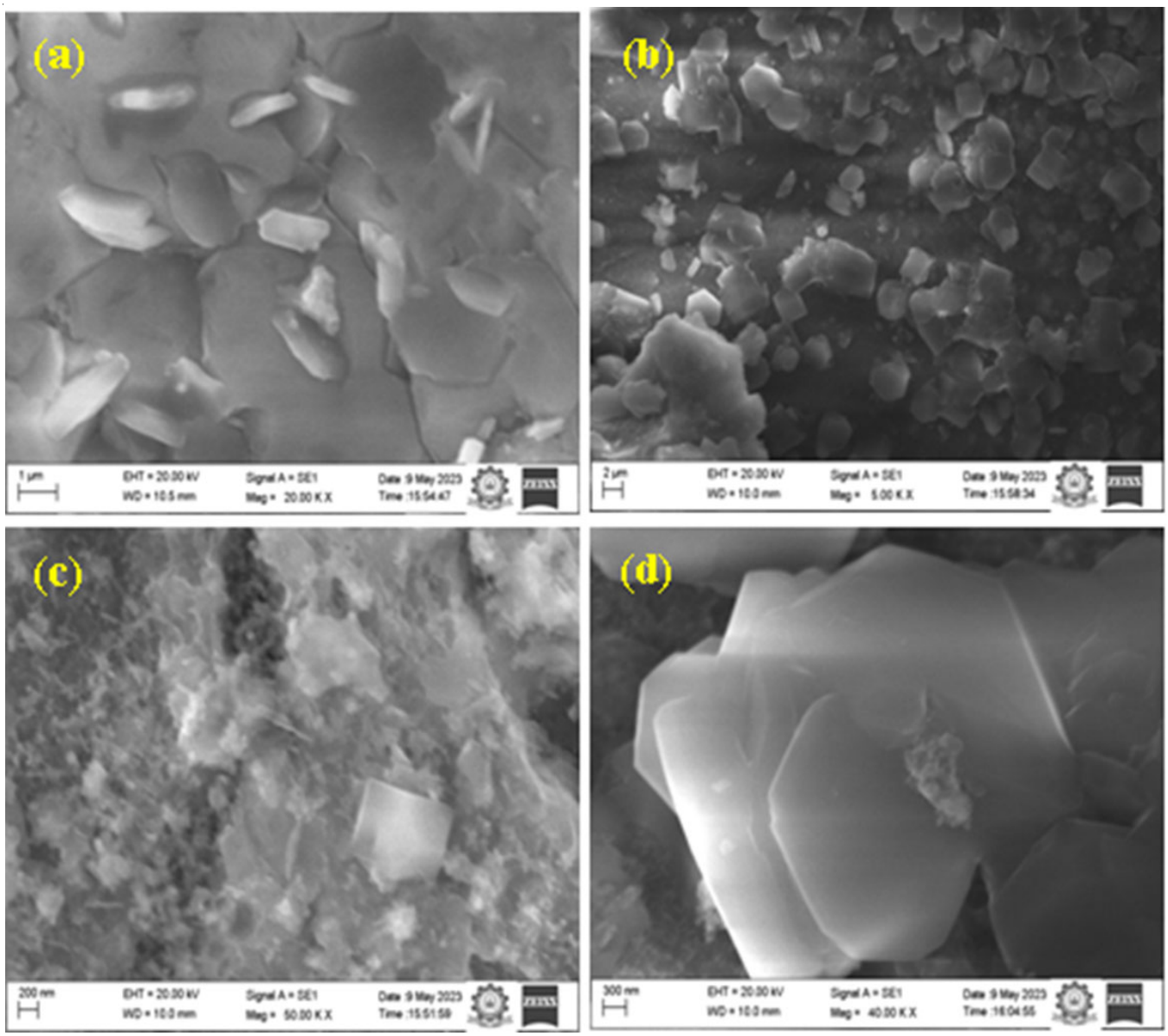

Fig. 2. FE-SEM images of SP-$CdFe_2O_4$ at (a) 1 µm (b) 2 µm and (c) 200 nm and (d) 300 nm

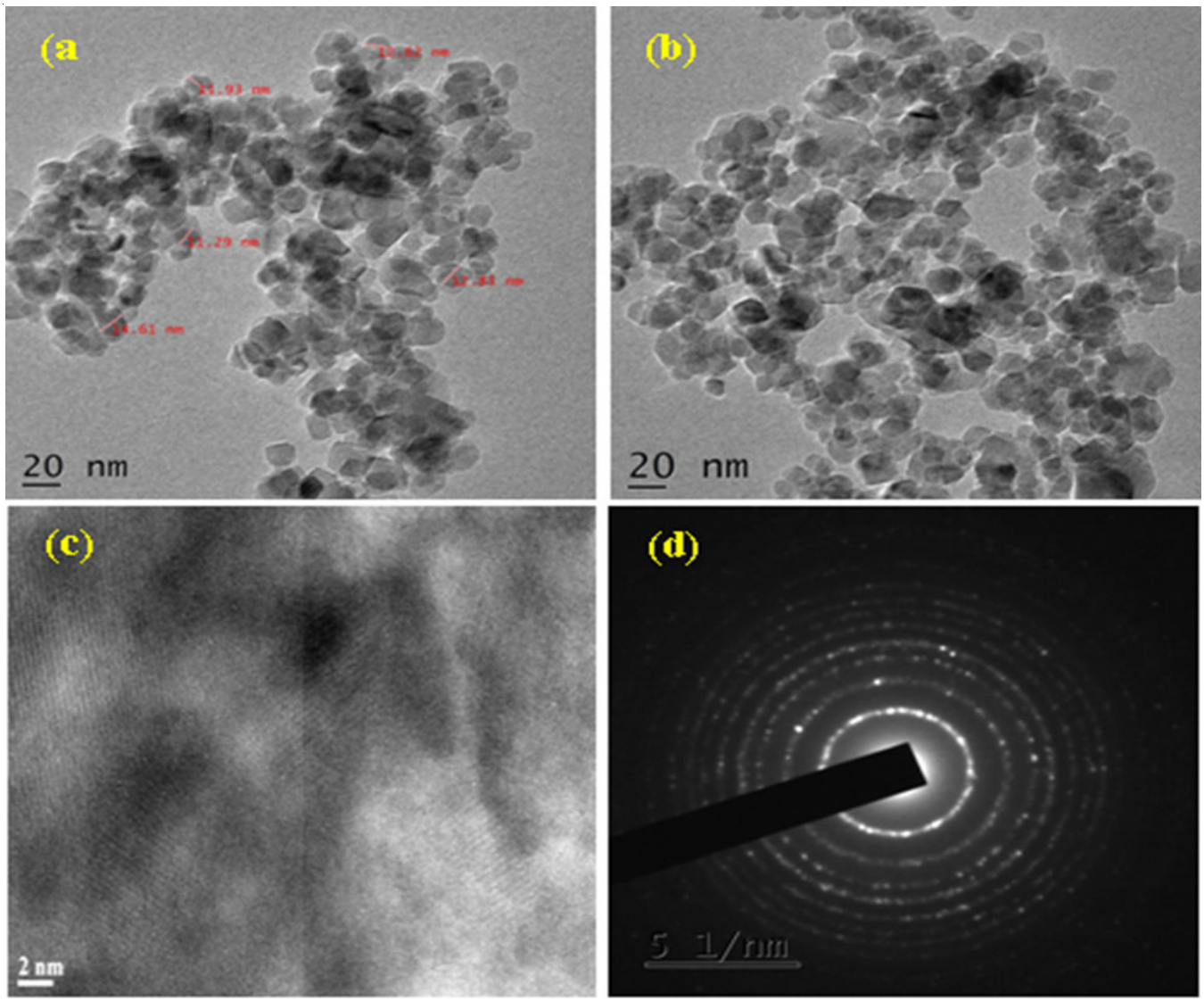

Fig. 3. HR-TEM images of sepiolite/$CdFe_2O_4$ (a, b) 20 nm, (c) lattice fringes at 2 nm and (d) SAED pattern of sepiolite/$CdFe_2O_4$ at 5 1/nm

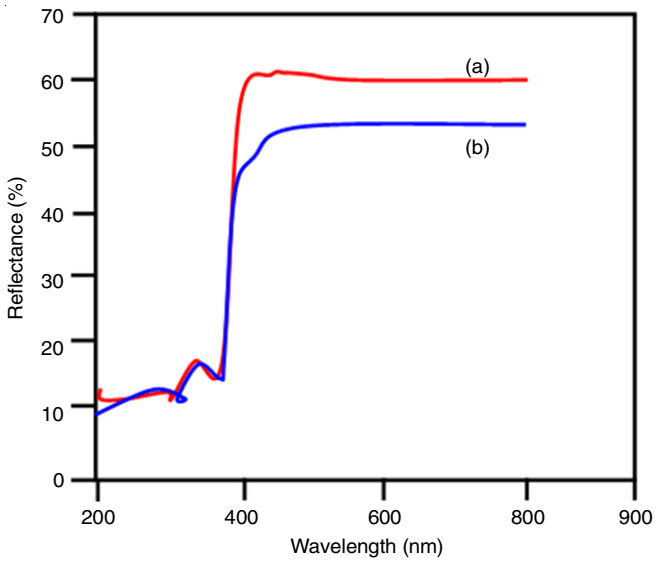

Fig. 4. Diffuse reflectance spectra of (a) prepared $CdFe_2O_4$ and (b) 5 wt% sepiolite/$CdFe_2O_4$

Photoluminescence (PL) studies: The PL spectrum of 5 wt.% sepiolite/$CdFe_2O_4$ at an excitation wavelength of 315 nm shows a sharp peak at ~430 nm, which is due to the emission of the host nanoparticles and another broad peak between 480 to 500 nm, which might be due to defects present in the nano-system. The PL emission is caused by the recombination of photoinduced charge carriers and shown a significant correlation between the intensity of PL emissions and photocatalytic activity. The photoluminescence spectra of prepared $CdFe_2O_4$ (a) and 5 wt.% sepiolite/$CdFe_2O_4$ (b) are shown in Fig. 5 (exi = 315 nm). In comparison to $CdFe_2O_4$, the reduced PL intensity of 5 wt.% sepiolite/$CdFe_2O_4$ indicates that the incorporation of sepiolite clay hinders the recombination of photogenerated electron-hole pairs.

BET surface area: Using nitrogen adsorption-desorption isotherms, the pore structure of sepiolite/$CdFe_2O_4$ composite sample was examined and the Barrett-Joyner-Halenda (BJH) method was utilized to compute the pore size distribution. There is a significant rise in the N_2 adsorption volume, which is found

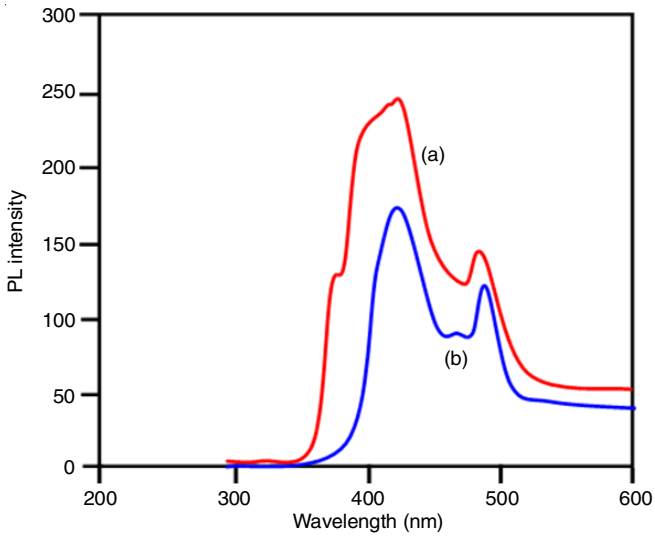

Fig. 5. Photoluminescence spectra of (a) prepared $CdFe_2O_4$ and (b) 5 wt% sepiolite/ $CdFe_2O_4$.

in the 0.50-0.98 P/P_0 range (Fig. 6). Since, the pore size is related to the P/P_0 position of inflection point, this abrupt increase can be attributed to the capillary condensation, showing strong homogeneity of the sample and mesopore size. The pore size distribution curve in the inset figure illustrates the average pore radius of sepiolite/$CdFe_2O_4$ as 126 Å. The mesoporous structure is thus confirmed by the pore size distribution of sepiolite/$CdFe_2O_4$ sample. The BET measurements of $CdFe_2O_4$ yield a specific surface area of 18.94 $m^2 g^{-1}$, which is greater than the prepared sepiolite/$CdFe_2O_4$'s 36.48 $m^2 g^{-1}$.

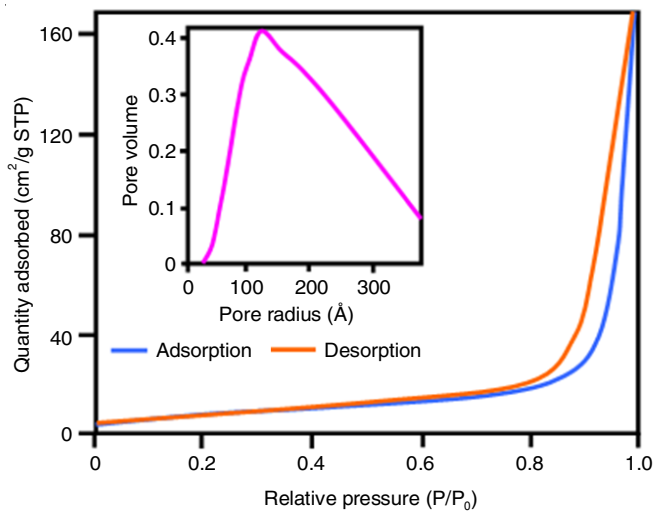

Fig. 6. BET surface analysis of sepiolite/$CdFe_2O_4$ N_2 adsorption-desorption isotherm and (inset) Pore radius distribution

Photodegradation of rhodamine-B (Rh-B) dye under solar light

Fig. 7 illustrates the photocatalytic breakdown of Rh-B dye under various conditions and increasing irradiation times. Since the dye is resistant to self-photolysis, a slight (10%) drop in dye concentration was observed in the same experiment with sepiolite/$CdFe_2O_4$ in dark. At 45 min exposure of sunlight,

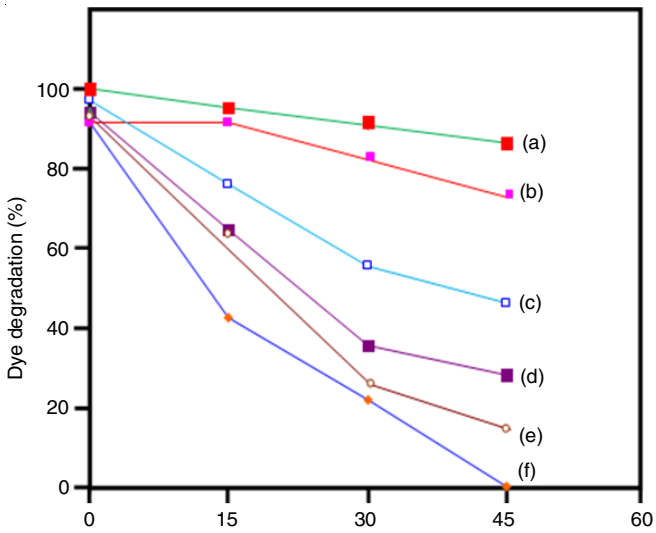

Fig. 7. Rh-B dye degradation: dye concentration = 3×10^{-4} M, (a) Rh-B dye, (b) Rh-B + CdO, (c) Rh-B + sepiolite, (d) Rh-B + $CdFe_2O_4$, (e) Rh-B + 3 wt.% of sepiolite/$CdFe_2O_4$ and (f) Rh-B + 5 wt.% of sepiolite/$CdFe_2O_4$

sepiolite/$CdFe_2O_4$ cause 99% degradation of Rh-B dye. There are no specific changes in dark (curve a) or without a catalyst (curve b). But at 45 min, sepiolite clay (curve c), $CdFe_2O_4$ (curve d) and 3 wt.% sepiolite/$CdFe_2O_4$ (curve e) generated degradations of 37.7%, 60.2% and 78.3%, respectively. When it combined with 5 wt.% of sepiolite/$CdFe_2O_4$ the dye was completely degraded (curve f).The results clearly demonstrate that the loaded sepiolite clay is responsible for the increased photocatalytic activity.

Photodegradation efficiency with solar light: The photodegradation efficiencies of sepiolite/$CdFe_2O_4$ catalysts with 3, 5 and 9 wt.% sepiolite were also evaluated under solar light. Catalysts containing 5 wt.% sepiolite demonstrated the highest degradation percentage, while higher sepiolite concentrations resulted in decreased degradation efficiency (Table-1). Therefore, 5 wt.% sepiolite was identified as the optimal concentration for sepiolite/$CdFe_2O_4$. Since 5 wt.% of sepiolite/$CdFe_2O_4$ was found to be most efficient in solar light for the degradation of Rh-B dye.

TABLE-1
EFFECT OF DIFFERENT wt.% OF SEPIOLITE/$CdFe_2O_4$ ON THE DEGRADATION OF Rh-B DYE UNDER SOLAR LIGHT IRRADIATION

Wt.% of sepiolite	Degradation percentage of Rh-B
3	45.2
5	99.4
9	59.5

Rh-B dye concentration = 3×10^{-4} M, catalyst suspended = 3 g L^{-1}, pH = 7 airflow rate = 8.1 mL s^{-1}, irradiation time = 45 min, I_{solar} = 1250 ×100 ± 100 lx

Effect of solution pH: In the pH range of 3 to 11, the impact of pH on Rh-B dye photodegradation was investigated. At pH 3, 5, 7, 9 and 11, respectively, the percentages of Rh-B degradation after 45 min of irradiation are 42.1, 58.5, 99.5, 76.6 and 63.5% (Fig. 8). As the pH attains the neutral range

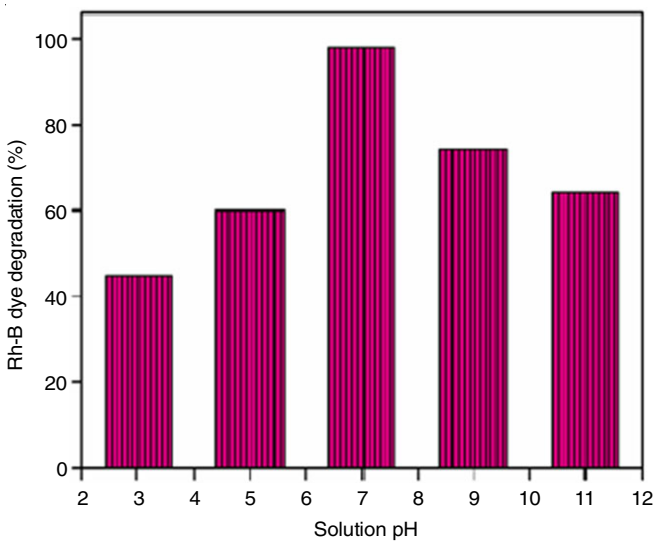

Fig. 8. Effect of solution pH on Rh-B degradation: dye concentration = 3 × 10^{-4} M, catalyst suspended = 3 g L^{-1}, airflow rate = 8.1 mL s^{-1}, irradiation time = 45 min, I_{solar} = 1250 × 100 ± 100 lx

(pH 7), the degradation efficiency decreases. Thus, at pH 7, there is elevated absorption and enhanced photocatalytic activity in the breakdown of Rh-B dye molecules.

Effect of nanocomposite loading: The effectiveness of sepiolite/$CdFe_2O_4$ as catalyst in varying quantities is shown in Fig. 9. Consequently, it suggests that in comparison to other concentrations, nanocomposite with 3 g L^{-1} exhibits the highest photodegradation under solar light energy. The amount of molecules adsorbed onto the surface of nanocomposite is generally believed to have a relationship with the efficiency of a photocatalyst. Lower activity over 3 g L^{-1} photocatalysis is caused by the agglomeration of catalyst.

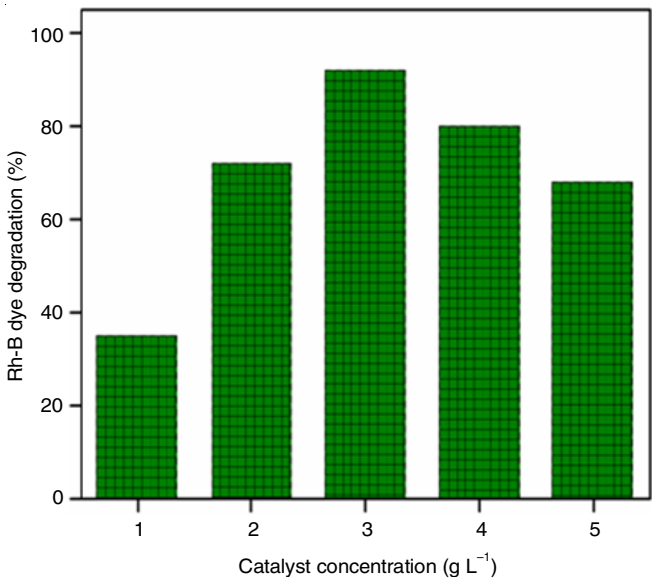

Fig. 9. Effect of catalyst loading on Rh-B degradation: dye concentration = 3 × 10^{-4} M, pH = 7, catalyst suspended = 3 g L^{-1}, airflow rate = 8.1 mL s^{-1}, irradiation time = 45 min, I_{solar} = 1250 × 100 ± 100 lx

Reusability of catalyst: Reusability studies could confirm the strength and activity efficiency of photocatalysts. As the Rh-B dye molecule breaks down, Fig. 10 displays the reusability result of sepiolite/$CdFe_2O_4$.The catalyst was repeatedly purified using ethanol and water after it had been filtered and isolated from the dye solution after the degradation process was finished. After drying at 100 ºC, the catalyst was put to further analysis. The photocatalytic activity was stable with the Rh-B dye in solution completely decomposed during 45 min irradiation for each cycle, though a small decline (< 8%) can be detected after four cycles.

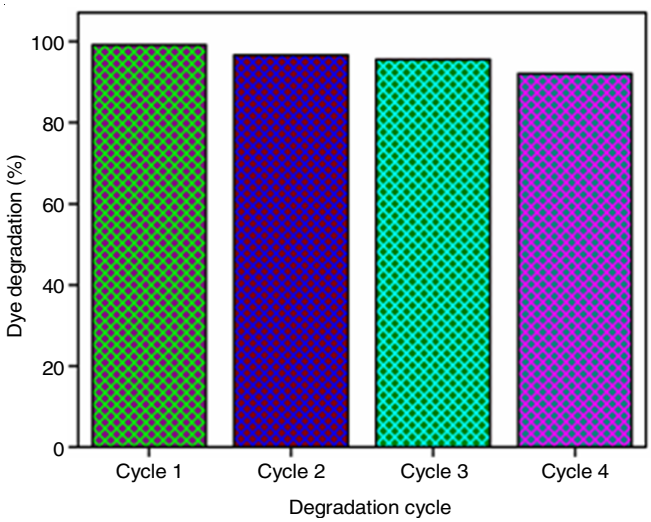

Fig. 10. Reusability of sepiolite/$CdFe_2O_4$ nanocomposite on Rh-B degradation: dye concentration = 3 × 10^{-4} M, pH = 7, catalyst suspended = 3 g L^{-1}, airflow rate = 8.1 mL s^{-1}, irradiation time = 45 min, I_{solar} = 1250 × 100 ± 100 lx

Mechanism of degradation: As mentioned, the heterostructures consist of well-interacted CdO and Fe_2O_3 nanoparticles deposited as $CdFe_2O_4$ on the surface of sepiolite clay material. **Scheme-I** proposes the separation and transportation of electron-hole pairs at the interface between the CdO and Fe_2O_3 photocatalysts. The electron-hole pairs are produced by photogenerated CdO. Since CdO has a higher CB position than

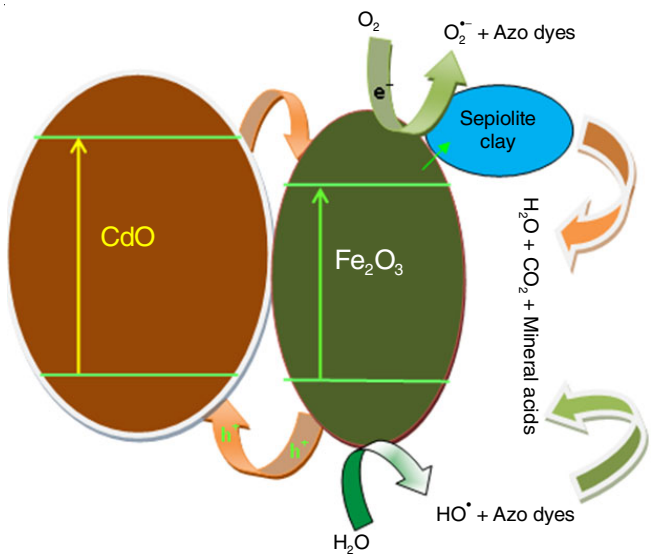

Scheme-I: Photodegradation mechanism of sepiolite/$CdFe_2O_4$

Fe_2O_3, photogenerated electrons on CdO can directly inject into Fe_2O_3's CB band. This increases the efficiency of charge separation and lowers the likelihood of recombination, which boosts photocatalytic activity. Loaded sepiolite clay also contains a large number of metal and non-metal oxides in addition to this electron transfer. Metal ions function as electron sinks to lessen electron-hole recombination and can create sporadic energy levels to lower band gap energy.

Contact angle measurements: The water contact angle (WCA) reflects the surface non-wettability of prepared catalyst. To assess the hydrophobicity of catalyst, the contact angles of glass slides coated with TEOS, TEOS + $CdFe_2O_4$, TEOS + sepiolite clay and TEOS + sepiolite/$CdFe_2O_4$ were measured. Fig. 11 presents the water contact angles for these four different coatings: TEOS + $CdFe_2O_4$ (b), TEOS + sepiolite clay (c), with a measured angle of 108.3º for TEOS + sepiolite/$CdFe_2O_4$ (d) and 22.5º for the untreated glass slide (a). The increased fraction of air/water contact on a rough surface can enhance super hydrophobicity, indicating that sepiolite/$CdFe_2O_4$ coating exhibits greater hydrophobicity. Consequently, this property transforms the catalyst into a self-cleaning material, leading to reduced surface wettability.

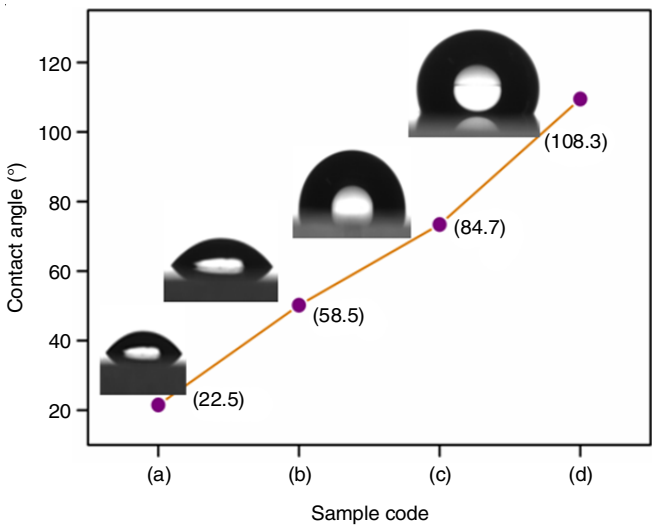

Fig. 11. Water contact angle of different samples (a) uncoated glass slide, (b) TEOS + $CdFe_2O_4$ coated glass slide, (c) TEOS + sepiolite clay coated glass slide and (d) TEOS + sepiolite/$CdFe_2O_4$ coated glass slide

Conclusion

The hydrothermal co-precipitation approach was used to synthesize $CdFe_2O_4$ supported by sepiolite without the use of organic solvents or surfactants. The FE-SEM images revealed that the synthesized sepiolite/$CdFe_2O_4$ has a loosely clustered sandwich-like microstructure, whereas the HR-TEM analysis confirmed the presence of numerous regular-shaped, hollow spherical particles, providing additional evidence of uniform coating of $CdFe_2O_4$ nanoparticles on the sepiolite clay surface. The photodegradation tests demonstrated that 5 wt.% sepiolite supported $CdFe_2O_4$ is significantly more effective at degrading rhodamine-B dye at neutral pH 7. The reduced fluorescence intensity of sepiolite/$CdFe_2O_4$ indicates decreased recombination of electron-hole pairs. Additionally, the BET surface area of sepiolite/$CdFe_2O_4$ is higher at 36.48 m^2/g, compared to 18.94 m^2/g for $CdFe_2O_4$ alone. The water contact angle of 108.3º confirms the excellent hydrophobicity of sepiolite/$CdFe_2O_4$. This research emphasizes a new utilization of naturally occurring sepiolite in semiconductor oxide materials for energy and environmental applications.

ACKNOWLEDGEMENTS

The authors thank The Principal, Kalaignar Karunanidhi Government Arts College and Department of Chemistry for their support and for providing a facilities for research.

CONFLICT OF INTEREST

The authors declare that there is no conflict of interests regarding the publication of this article.

REFERENCES

1. O. Silva and P.C. Morais, *J. Magn. Magn. Mater.*, **289**, 136 (2005); https://doi.org/10.1016/j.jmmm.2004.11.040
2. M. Yokoyama, E. Ohta, T. Sato and T. Sato, *J. Magn. Magn. Mater.*, **183**, 173 (1998); https://doi.org/10.1016/S0304-8853(97)01073-1
3. P. Singh, K. Sharma, V. Hasija, V. Sharma, S. Sharma, P. Raizada, M. Singh, A.K. Saini, A. Hosseini-Bandegharaei and V.K. Thakur, *Mater. Today Chem.*, **14**, 100186 (2019); https://doi.org/10.1016/j.mtchem.2019.08.005
4. X. Li, J. Wang, J. Zhang, C. Zhao, Y. Wu and Y. He, *J. Colloid Interface Sci.*, **607**, 412 (2022); https://doi.org/10.1016/j.jcis.2021.09.004
5. Z. Li, Q. Zhang, L. Wang, J. Yang, Y. Wu and Y. He, *Ultrason. Sonochem.*, **78**, 105729 (2021); https://doi.org/10.1016/j.ultsonch.2021.105729
6. A. Amirnasiri and S.E. Mirsalehi, *Ceram. Int.*, **47**, 34414 (2021); https://doi.org/10.1016/j.ceramint.2021.08.354
7. S. Gunes, K.P. Fritz, H. Neugebauer, N.S. Sariciftci, S. Kumar and G.D. Scholes, *Sol. Energy Mater. Sol. Cells*, **91**, 420 (2007); https://doi.org/10.1016/j.solmat.2006.10.016
8. C. Rumenapp, B. Gleich and A. Haase, *Pharm. Res.*, **29**, 1165 (2012); https://doi.org/10.1007/s11095-012-0711-y
9. R. Viswanath, H.S. Bhojya Naik, G. Arun Kumar, I.K. Suresh Gowda and S. Yallappa, *Luminescence*, **32**, 1212 (2017); https://doi.org/10.1002/bio.3313
10. P. Srinoi, Y.-T. Chen, V. Vittur, M.D. Marquez and T.R. Lee, *Appl. Sci.*, **8**, 1106 (2018); https://doi.org/10.3390/app8071106
11. J.Z. Msomi, *J. Magn. Magn. Mater.*, **336**, 61 (2013); https://doi.org/10.1016/j.jmmm.2013.02.021
12. Z. Sun, L. Liu, D. Jia and W. Pan, *Sens. Actuators B Chem.*, **125**, 144 (2007); https://doi.org/10.1016/j.snb.2007.01.050
13. A.V. Raut, R.S. Barkule, D.R. Shengule and K.M. Jadhav, *J. Magn. Magn. Mater.*, **358–359**, 87 (2014); https://doi.org/10.1016/j.jmmm.2014.01.039
14. E.R. Kumar, R. Jayaprakash, G.S. Devi and P.S.P. Reddy, *J. Magn. Magn. Mater.*, **355**, 87 (2014); https://doi.org/10.1016/j.jmmm.2013.11.051
15. E.H. Kim, H.S. Lee, B.K. Kwak and B.-K. Kim, *J. Magn. Magn. Mater.*, **289**, 328 (2004); https://doi.org/10.1016/j.jmmm.2004.11.093
16. D. Ramimoghadam, S. Bagheri and S.B.A. Hamid, *J. Magn. Magn. Mater.*, **368**, 207 (2014); https://doi.org/10.1016/j.jmmm.2014.05.015
17. O.M. Hemeda, N.Y. Mostafa, O.H.A. Elkader and M.A. Ahmed, *J. Magn. Magn. Mater.*, **364**, 39 (2014); https://doi.org/10.1016/j.jmmm.2014.03.061

18. R.M. Mohamed, M.M. Rashad, F.A. Haraz and W. Sigmund, *J. Magn. Magn. Mater.*, **322**, 2058 (2010); https://doi.org/10.1016/j.jmmm.2010.01.034
19. M. Houshiar, F. Zebhi, Z.J. Razi, A. Alidoust and Z. Askari, *J. Magn. Magn. Mater.*, **371**, 43 (2014); https://doi.org/10.1016/j.jmmm.2014.06.059
20. P. Pulisova, J. Kovac, A. Voigt and P. Raschman, *J. Magn. Magn. Mater.*, **341**, 93 (2013); https://doi.org/10.1016/j.jmmm.2013.04.003
21. I. Sharifi, H. Shokrollahi, M. Doroodmand and R. Safi, *J. Magn. Magn. Mater.*, **324**, 1854 (2012); https://doi.org/10.1016/j.jmmm.2012.01.015
22. M. Zhang, Z. Zi, Q. Liu, X. Zhu, C. Liang, Y. Sun and J. Dai, *J. Magn. Magn. Mater.*, **369**, 23 (2014); https://doi.org/10.1016/j.jmmm.2014.06.019
23. M.E. Arani, M.J.N. Isfahani and M.A. Kashi, *J. Magn. Magn. Mater.*, **322**, 2944 (2010); https://doi.org/10.1016/j.jmmm.2010.05.010
24. Z. Karcioglu Karakas, R. Boncukcuoglu, I.H. Karakas and M. Ertugrul, *J. Magn. Magn. Mater.*, **374**, 298 (2015); https://doi.org/10.1016/j.jmmm.2014.08.045
25. W. Liu, C. Zhao, S. Wang, L. Niu, Y. Wang, S. Liang and Z. Cui, *Res. Chem. Intermed.*, **44**, 1441 (2018); https://doi.org/10.1007/s11164-017-3178-y
26. A. Heydari and H. Sheibani, *RSC Adv.*, **5**, 82438 (2015); https://doi.org/10.1039/C5RA12423A
27. A. Heydari, H. Khoshnood, H. Sheibani and F. Doostan, *Polym. Adv. Technol.*, **28**, 524 (2017); https://doi.org/10.1002/pat.3951
28. L.X. Zhu, J.S. Guo, P. Liu and S.B. Zhao, *Appl. Clay Sci.*, **121-122**, 29 (2016); https://doi.org/10.1016/j.clay.2015.12.020
29. T.P.A. Shabeer, A. Saha, V.T. Gajbhiye, S. Gupta, K.M. Manjaiah and E. Varghese, *Water Air Soil Pollut.*, **226**, 41 (2015); https://doi.org/10.1007/s11270-015-2331-8
30. V. Marjanovic, S. Lazarevic, I. Jankovic-Castvan, D. Janackovic, B. Jokic and R. Petrovic, *Appl. Clay Sci.*, **80-81**, 202 (2013); https://doi.org/10.1016/j.clay.2013.04.008
31. E.I. Unuabonah, K.O. Adebowale and B.I. Olu-Owolabi, *J. Hazard. Mater.*, **144**, 386 (2007); https://doi.org/10.1016/j.jhazmat.2006.10.046
32. Z.H. Siahpoosh and M. Soleimani, *Bioanal. Chem. Res.*, **3**, 195 (2016); https://doi.org/10.22036/abcr.2016.16482
33. R. Donat, *J. Chem. Thermodyn.*, **41**, 829 (2009); https://doi.org/10.1016/j.jct.2009.01.009
34. M. Suárez and E. García-Romero, *Appl. Clay Sci.*, **67–68**, 72 (2012); https://doi.org/10.1016/j.clay.2012.06.003
35. Y. Yu, S. Qi, J. Zhan, Z. Wu, X. Yang and D. Wu, *Mater. Res. Bull.*, **46**, 1593 (2011); https://doi.org/10.1016/j.materresbull.2011.06.009
36. Y. Zheng and Y. Zheng, *J. Appl. Polym. Sci.*, **99**, 2163 (2006); https://doi.org/10.1002/app.22337
37. O. Ozdemir, M. Cinar, E. Sabah, F. Arslan and M.S. Celik, *J. Hazard. Mater.*, **147**, 625 (2007); https://doi.org/10.1016/j.jhazmat.2007.01.059
38. S. Hojati and H. Khademi, *J. Cent. South Univ.*, **20**, 3627 (2013); https://doi.org/10.1007/s11771-013-1889-9
39. S. Sagadevan, K. Pal, Z.Z. Chowdhury and M.E. Hoque, *Mater. Res. Express*, **4**, 075025 (2017); https://doi.org/10.1088/2053-1591/aa77b5
40. C. Reitz, C. Suchomski, V.S.K. Chakravadhanula, I. Djerdj, Z. Jaglièic and T. Brezesinski, *Inorg. Chem.*, **52**, 3744 (2013); https://doi.org/10.1021/ic302283q
41. K. Brezesinski, J. Haetge, J. Wang, S. Mascotto, C. Reitz, A. Rein, S.H. Tolbert, J. Perlich, B. Dunn and T. Brezesinski, *Small*, **7**, 407 (2011); https://doi.org/10.1002/smll.201001333